BJC

Assessing vascular effects of adding bevacizumab to neoadjuvant chemotherapy in osteosarcoma using DCE-MRI

J Guo*,[1], J O Glass[1], M B McCarville[1], B L Shulkin[1], V M Daryani[2], C F Stewart[2], J Wu[3], S Mao[3], J R Dwek[4], L M Fayad[5], J E Madewell[6], F Navid[7,8], N C Daw[7,9] and W E Reddick[1]

[1]Department of Diagnostic Imaging, St Jude Children's Research Hospital, 262 Danny Thomas Place, Mail Stop 220, Memphis, TN 38105-3678, USA; [2]Department of Pharmaceutical Sciences, St Jude Children's Research Hospital, Memphis, TN 38105, USA; [3]Department of Biostatistics, St Jude Children's Research Hospital, Memphis, TN 38105, USA; [4]Department of Radiology, Rady Children's Hospital, San Diego, CA 92123, USA; [5]The Musculoskeletal Tumor Program, The Johns Hopkins University, Baltimore, MD 21287, USA; [6]Department of Diagnostic Radiology, The University of Texas MD Anderson Cancer Center, Houston, TX 77030, USA; [7]Department of Oncology, St Jude Children's Research Hospital, Memphis, TN 38105, USA; [8]Department of Pediatrics, College of Medicine, University of Tennessee Health Science Center, Memphis, TN 38163, USA and [9]Division of Pediatrics, The University of Texas MD Anderson Cancer Center, Houston, TX 77030, USA

Background: The purpose of this study was to assess the impact of bevacizumab alone and in combination with cytotoxic therapy on tumour vasculature in osteosarcoma (OS) using DCE-MRI.

Methods: Six DCE-MRI and three ^{18}F-FDG PET examinations were scheduled in 42 subjects with newly diagnosed OS to monitor the response to antiangiogenic therapy alone and in combination with cytotoxic therapy before definitive surgery (week 10). Serial DCE-MRI parameters (K^{trans}, v_p, and v_e) were examined for correlation with FDG-PET (SUV_{max}) and association with drug exposure, and evaluated with clinical outcome.

Results: K^{trans} ($P = 0.041$) and v_p ($P = 0.001$) significantly dropped from baseline at 24 h after the first dose of bevacizumab alone, but returned to baseline by 72 h. Greater exposure to bevacizumab was correlated with larger decreases in v_p at day 5 ($P = 0.04$) and week 10 ($P = 0.02$). A lower K^{trans} at week 10 was associated with greater percent necrosis ($P = 0.024$) and longer event-free survival ($P = 0.034$).

Conclusions: This is the first study to demonstrate significant changes of the plasma volume fraction and vascular leakage in OS with bevacizumab alone. The combination of demonstrated associations between drug exposure and imaging metrics, and imaging metrics and patient survival during neoadjuvant therapy, provides a compelling rationale for larger studies using DCE-MRI to assess vascular effects of therapy in OS.

Osteosarcoma (OS) is the most common malignant bone tumour in children. The current treatment strategy of neoadjuvant chemotherapy followed by surgical resection of the primary tumour and postoperative chemotherapy yields a long-term survival rate of ~60% to 70% in patients with localised disease and <30% in those with metastatic disease at diagnosis (Rosen

et al, 1979; Bacci et al, 2001; Longhi et al, 2006). Unfortunately, with no new cytotoxic agents available, survival rates have remained unchanged over the past two decades.

Antiangiogenic agents have shown promise in treating solid cancers and are known to be more effective when combined with cytotoxic therapy (Jain, 2005a, b; Dickson et al, 2007). Tumour

vasculature can be tortuous, causing irregular blood flow and high interstitial fluid pressures that may impair the delivery of oxygen and cytotoxic agents to the tumour. Bevacizumab, a monoclonal antibody targeting vascular endothelial growth factor A (VEGF-A), is thought to prune tumour blood vessels, thus normalising structure and improving oxygenation and drug delivery (Shih and Lindley, 2006). However, bevacizumab can cause additional loss of blood vessels that would hinder the delivery of therapy. Understanding the time course of these changes in OS would aid in determining the optimum time to deliver the cytotoxic agents. Therefore, noninvasive methods that can monitor tumour vascular changes could be critical for the management of patients during neoadjuvant therapy with bevacizumab.

Imaging modalities commonly used to assess OS during neoadjuvant therapy include MRI and positron emission tomography (PET). Dynamic contrast-enhanced MRI (DCE-MRI) is used to measure properties of tissue microvasculature, such as tissue perfusion, capillary permeability, and interstitial volume (Tofts *et al*, 1999; Verstraete and Lang, 2000). Dynamic contrast-enhanced MRI monitors signal changes during and after the intravenous injection of a gadolinium contrast agent. Regions of necrosis, muscle, vessel, and viable tumour display distinct signal enhancement in dynamic images. Dynamic contrast-enhanced MRI is widely used in clinical studies for the assessment of treatment response and as a potential prognostic biomarker for histologic response and survival in children with OS (Reddick *et al*, 1999, 2001; Dyke *et al*, 2003; Hoang *et al*, 2004; Bajpai *et al*, 2011; Guo *et al*, 2012; Amit *et al*, 2014). Positron emission tomography with ^{18}F-FDG, an analogue of glucose, also generates measures that can be used for staging, and monitoring of response in OS (Ye *et al*, 2008; Cheon *et al*, 2009; Hawkins *et al*, 2009).

The purpose of this study was to assess the impact of bevacizumab alone and in combination with cytotoxic therapy on tumour vasculature in pediatric OS patients treated on a multi-institutional trial. Serial DCE-MRI kinetic parameters were compared with FDG-PET, explored for associations with bevacizumab and methotrexate (MTX) exposure, and evaluated with clinical end points of histologic response and survival.

MATERIALS AND METHODS

Patients and treatment. A total of 42 subjects (23 male and 19 female), younger than 30 years of age, with newly diagnosed, high-grade OS were enrolled on a phase II therapeutic trial at four medical centres in the United States between May 2008 and April 2012 (NCT00667342). The median age was 12.5 years at diagnosis. Thirty-one patients had localised, resectable disease and 11 patients had metastatic disease at diagnosis.

Neoadjuvant therapy consisted of two cycles of cisplatin, doxorubicin, and methotrexate administered over 10 weeks followed by gross total resection. Bevacizumab was administered 3 days before the first dose of chemotherapy at week 0 with subsequent doses given on day 1 of week 3 and week 5. Imaging modalities used to monitor response to treatment included DCE-MRI (all 42 subjects) and ^{18}F-FDG PET (34 subjects). The treatment and imaging schedules are shown in Figure 1. This study was approved by the institutional review board of the participating institutions, and written informed consent was obtained from the patient, parent or guardian, as appropriate.

Pharmacokinetics. The bevacizumab sampling strategy, sample analysis, and development of the population pharmacokinetic model have been previously described (Turner *et al*, 2014). Bevacizumab concentration–time data were fit to a two-compartment model with first-order elimination from the central compartment. Bevacizumab exposure (area under curve (AUC))
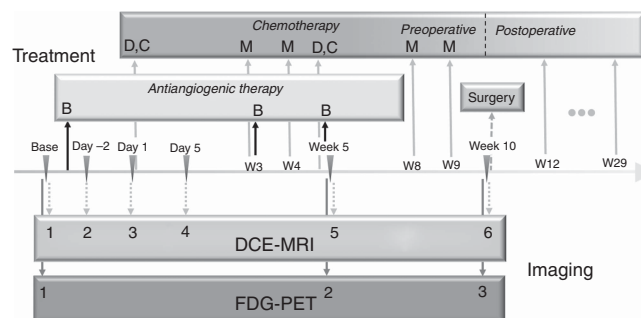

Figure 1. Treatment schema and timing of DCE-MRI and PET imaging. Base represents the baseline for both MRI and PET; day -2 represents the time point 1 day after bevacizumab; day 1 represents the time point just before administration of chemotherapy (3 days after bevacizumab); day 5 represents the time point $\sim$7 days after bevacizumab. B = bevacizumab; C = cisplatin; D = doxorubicin; M = methotrexate; W = week.

from the first dose to time of imaging was calculated for each patient in NONMEM (version 7.3; ICON Solutions, Hanover, MD, USA).

Methotrexate pharmacokinetic studies were performed in 33 patients for clinical monitoring purposes with samples routinely collected at 4, 24, 48, and 72 h post infusion. Serum MTX concentrations were fit to a two-compartment first-order elimination model using ADAPT II (Biomedical Simulations Resource, University of Southern California, Los Angeles, CA, USA) (Crews *et al*, 2004). The MTX AUC was determined by taking each patient's MTX dosage divided by the *post hoc* BSA normalised clearance and used to calculate the MTX average AUC (AUC_{avg}) of week 3 and week 4 doses.

Imaging protocols. For each subject, six serial DCE-MRI examinations were scheduled (Figure 1): at baseline (before the first bevacizumab administration), on day -2 (1 day after the first bevacizumab administration), on day 1 (3 days after bevacizumab on the day of chemotherapy administration), day 5 (7 days after bevacizumab), at week 5, and at week 10 before tumour resection. To evaluate the effect of bevacizumab alone, the first bevacizumab administration was administered 3 days before the first chemotherapy administration, and chemotherapy was not administered until after the DCE-MRI examination on day 1. For subjects enrolled at the primary institution ($n = 27$), three serial ^{18}F-FDG PET/CT examinations were acquired at baseline before any treatment and week 5 and week 10.

DCE-MRI acquisition and processing. The DCE-MRI data were acquired on 1.5 T MRI scanners (Avanto; Siemens Medical Solutions, Erlangen, Germany; Signa HDxt; GE Healthcare, Milwaukee, WI, USA) using torso and spine coil arrays. The baseline spin lattice relaxation time T_{10} was measured before each DCE-MRI scan using the inversion recovery method (inversion times = 100, 300, 900, 1500, 2200, and 3300 ms; 16 slices with 5 mm thickness; FOV and position matched to DCE-MRI acquisition; TR/TE = 4000/78 ms). Subjects were given intravenous injections of 0.1 mmol kg^{-1} of a gadolinium contrast (Magnevist Bayer Schering Pharma AG, Berlin-Wedding, Germany) at a constant rate of 1 ml s^{-1}, followed by a saline flush using a power injector synchronised with the MRI scanner. The DCE-MRI data were acquired using a fast 3D Cartesian gradient-echo pulse sequence with radiofrequency spoiling (16 slices with 5 mm thickness; 75% partial Fourier slice encoding; FOV kept same for each subject; TE/TR = 1.24/3.5 ms). Total acquisition time was 350 s for 50 measurements for a temporal resolution of 7 s for each measurement.

The DCE-MRI images were transferred to an offline work-station where a pediatric radiologist (MBM) used an interactive

display to select the region of interest (ROI) on each slice and ensured tumour boundary selection was consistent across all time points. Data were then analysed using a two-compartment pharmacokinetic model (Tofts *et al*, 1999) that required an arterial input function (AIF) and the baseline spin-lattice relaxation time (T_{10}). A modified experimentally derived AIF (Parker *et al*, 2006) was used because a measured AIF was not evaluable for all subjects. The fitting of the pharmacokinetic model for each pixel produces three quantitative measures (K^{trans}, v_e, and v_p). Pearson's χ^2 test was used to evaluate the goodness of the fit and to exclude pixels with poor fitting in non-enhancing tissues. In this study, K^{trans}, the volume transfer constant, v_e, the fractional volume of extravascular extracellular space, and v_p, the fractional blood plasma volume, were used to evaluate clinical outcomes (Tofts and Kermode, 1991; Tofts *et al*, 1999). The average for the distribution of each quantitative measure across the whole ROI was calculated as a summary measure for each data set. In addition, the skewness, kurtosis, and P95 of each kinetic parameter in each tumour were computed to explore possible non-normality of the histograms and their relationship to response and survival. P95 denotes the level of each kinetic parameter exceeding 95% of its values in each tumour.

^{18}F-FDG PET acquisition and processing. Following an overnight fast, or minimum 4 h of fast for afternoon studies, patients were injected with 0.15 mCi kg^{-1} ^{18}F-FDG (maximum 12 mCi) intravenously. Patients were kept in a quiet dark room after injection and encouraged to remain recumbent and relaxed. Transmission CT images for attenuation correction and lesion localisation, and PET emission images were acquired ~1 h later using a GE Discovery LS PET/CT system (GE Medical Systems, Waukesha, WI, USA). Following CT scanning for attenuation correction, PET images were obtained from the top of the skull through the feet for 5 min per bed position in 2D mode. After August 2011, images were acquired on a GE Discovery 690 PET CT device in 3D mode. Images were reconstructed using standard vendor-supplied software. In heterogeneous tumours such as OS, the highest single standardised uptake value (SUV_{max}) within the tumour is the most commonly used measure for describing the metabolism of the overall tumour. For each data set, SUV_{max} in the tumour was determined.

Evaluation of response and survival. Histologic response was assessed at week 10 after definitive surgery using the four-grade system of Huvos (Huvos *et al*, 1977; Rosen *et al*, 1982). Responders were defined as ≥90% necrosis (grade III 90–99% and grade IV 100%) and nonresponders as <90% (grade I 0–49% and grade II 50%–89%) (Wunder *et al*, 1998). Because the presence of metastatic diseases is an overwhelming factor in determining survival, only patients with localised disease were included in the analyses of event-free survival (EFS) and overall survival. Event-free survival was defined as the time interval from the date of study enrollment to the date of the first event (disease progression, relapse, secondary malignancy, or death) or to the date of last follow-up for patients without events. Overall survival was defined as the time from the date of study enrollment to the date of death from any cause or to the last follow-up date.

Statistical analysis. Nonparametric Wilcoxon signed-rank tests (Wilcoxon, 1945) were used to examine the difference of DCE-MRI parameters between any two time points. Nonparametric exact Wilcoxon rank-sum tests (Wilcoxon, 1945) were used to examine the difference of each parameter between responders and nonresponders. In all, 40 subjects for DCE-MRI and 32 subjects for PET were included in response analysis, and 2 subjects were excluded because one had a delayed surgery with additional chemotherapy and the other had an early surgery because of the progressive disease. Receiver-operating characteristic (ROC) curves were generated to compare K^{trans} and SUV_{max} at week 10 for

differentiating responders and nonresponders. Area under the curve, standard error (s.e.), 95% confidence interval (95% CI), and optimal cutoff were estimated in the ROC analyses. In addition, pairwise comparisons among three ROC curves were tested using the method of Delong *et al* (1988). Thirty-one patients with localised, non-metastatic disease at diagnosis were included in survival analyses. Cox proportional hazards models (Cox, 1972, 1975) were used to explore associations between outcome (EFS and overall survival) with each DCE-MRI parameter. Patients were categorised into two groups using the median K^{trans} parameter value at week 10 as a cut-point and EFS curves were estimated using the method of Kaplan and Meier (Kaplan and Meier, 1958) and differences in EFS curves were examined using the log-rank test (Bland and Altman, 2004). The DCE-MRI parameters were analysed against pharmacokinetic parameters using pair-wise Pearson's correlation tests. All statistical analyses were performed using SAS software (version 9.3, SAS Institute, Cary, NC, USA). Reported *P*-values were considered statistically significant when $P < 0.05$. No adjustments were made for multiple comparisons because of the exploratory nature of the analyses.

RESULTS

For the 42 subjects, DCE-MRI was acquired at baseline (in 35 patients), day −2 (27 patients), day 1 (27 patients), day 5 (32 patients), week 5 (38 patients), and week 10 (38 patients). Positron emission tomography examinations were completed at baseline (in 33 patients), week 5 (34 patients), and week 10 (32 patients). Bevacizumab and MTX pharmacokinetic studies were performed in 26 and 33 patients, respectively. Averaged DCE-MRI parameters (K^{trans}, v_p, and v_e) and PET parameter (SUV_{max}) at each time point are shown in box-and-whisker plots in Figure 2. To qualitatively appreciate DCE-MRI and PET in a responder and a nonresponder, images for two subjects are shown in Figure 3.

Imaging response to bevacizumab. The first three DCE-MRI imaging examinations (baseline, day −2, and day 1) were used to evaluate OS response to bevacizumab alone. These were acquired before the first bevacizumab administration and then 24 h (day −2) and 72 h (day 1) after administration. The 72 h imaging was acquired before cytotoxic chemotherapy was administered. Average v_e did not significantly differ from baseline at either day −2 or day 1. Average K^{trans} and v_p were both significantly lower than baseline values 24 h after bevacizumab administration (day −2, $P = 0.041$ and 0.001, respectively). However, 72 h after bevacizumab administration (day 1, start of cytotoxic therapy), these measures had increased and were no longer significantly different from baseline.

Imaging response to neoadjuvant therapy. Imaging measures during neoadjuvant therapy were evaluated at day 5, the mid-point (week 5), and completion of neoadjuvant therapy (week 10). The DCE-MRI parameters of average K^{trans} and v_p at weeks 5 and 10 were significantly lower and v_e at day 5 was significantly higher than baseline (*P*-values shown in Figure 2). A decrease in average v_p relative to baseline was correlated with increased bevacizumab exposure at day 5 ($AUC_{Day\ 5}$: $\rho = -0.44$, $P = 0.045$) and at week 10 ($AUC_{week\ 10}$: $\rho = -0.51$, $P = 0.027$). There was no significant correlation found between the decrease of K^{trans} and bevacizumab AUC at any time point. Increased MTX exposure was correlated with a decrease in K^{trans} at week 5 (AUC_{avg}: $\rho = -0.38$, $P = 0.0496$) and a decrease in v_p at week 10 (AUC_{avg}: $\rho = -0.50$, $P = 0.006$). In addition, a significant but moderate positive correlation was demonstrated between PET SUV_{max} and both DCE-MRI parameters at week 5 (average K^{trans}: $\rho = 0.56$, $P = 0.0007$; average v_p: $\rho = 0.43$, $P = 0.0135$) and average K^{trans} only at week 10 ($\rho = 0.51$, $P = 0.003$).
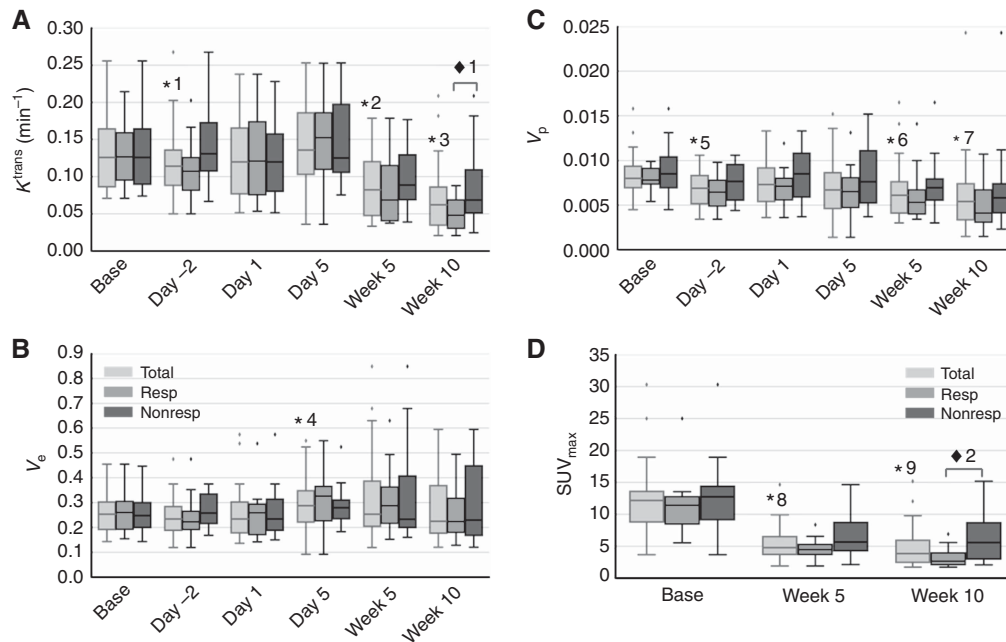
Figure 2. Box-and-whisker plots illustrate median values for DCE-MRI kinetic parameters (**A**) K^{trans}, (**B**) V_e, (**C**) V_p at six time points and PET SUV_{max} (**D**) at three time points. The asterisks (*) represent the significance of the difference between the measures and their corresponding baseline for all subjects. P-values of *1, *2, and *3 for K^{trans} are 0.041, <0.0001, and <0.0001, respectively; P-value of *4 for v_e is 0.027; P-values of *5, *6, and *7 for v_p are 0.0011, 0.0012, and <0.0001; P-values of *8 and *9 for SUV_{max} are <0.0001, respectively. The diamond (♦) represents the significant difference between responder and nonresponder groups. P-values of ♦1 for mean of K^{trans} at week 10 is 0.024; P values of ♦2 for SUV_{max} at week 10 is 0.012. NonResp = nonresponders; Resp = responders; Total = all subjects. The dots represent the outliers.
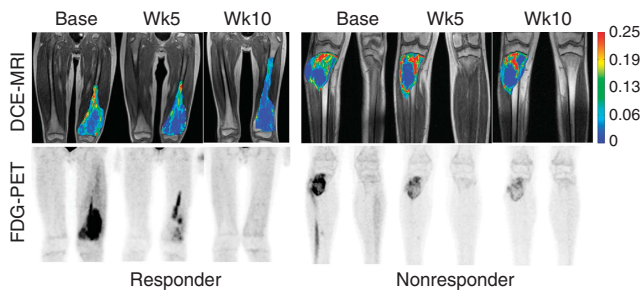

Figure 3. Comparison of DCE-MRI and FDG-PET images for two subjects: responder (left) and nonresponder (right). K^{trans} maps from a single central slice were overlaid on the corresponding greyscale image shown in the first row. Maximum intensity projection (MIP) images of SUV in the anterior–posterior direction were generated across the whole volume and shown in the second row. K^{trans} maps are in the same colour scale; and PET images are in the same greyscale.

Imaging and histologic response. Patients were categorised into two groups based on the Huvos grade of histologic response for DCE-MRI comparisons. Only average and P95 of K^{trans} and SUV_{max} at week 10 were significantly different between the two groups ($P = 0.024$, 0.024, and 0.012, respectively). The responders demonstrate lower K^{trans} rates and lower SUV_{max} values as shown in Figure 2A and D. The ROC curves of the average and P95 of K^{trans} and SUV_{max} at week 10 are shown in Figure 4. The AUCs from the three ROC curves were 0.71, 0.75, and 0.78, respectively. The corresponding s.e. were 0.085, 0.080, and 0.085. The corresponding 95% CIs were 0.55–0.88, 0.59–0.90, and 0.62–0.95. Although SUV_{max} demonstrated a slightly higher AUC than the two K^{trans}-based measures, there was no significant difference in pairwise comparisons between any of the three ROC curves
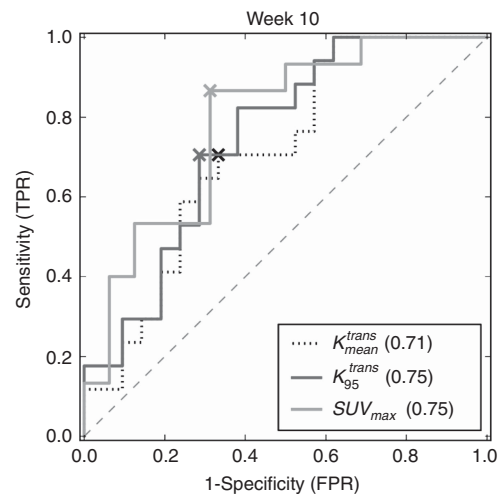

Figure 4. Receiver-operating characteristic (ROC) curves for K^{trans}_{mean}, K^{trans}_{95}, and SUV_{max} at week 10. The AUCs of the three ROC curves were 0.71, 0.75, and 0.78, respectively, in brackets. The corresponding cutoff values of K^{trans}_{mean}, K^{trans}_{95}, and SUV_{max} for 'X' markers were $0.054 \, min^{-1}$, $0.147 \, min^{-1}$, and 4.2, respectively. The corresponding sensitivities are 71%, 71%, and 87%, respectively. The corresponding specificities are 67%, 71%, and 69%, respectively. K^{trans}_{mean} represents the average of K^{trans}; K^{trans}_{95} represents the P95 of K^{trans}.

(all P-values >0.1). Optimal cutoff points were determined based on the ROC analysis of the averaged K^{trans} ($0.054 \, min^{-1}$), the P95 of K^{trans} ($0.147 \, min^{-1}$) and SUV_{max} (4.2).

Imaging and event-free and overall survival. For the 31 non-metastatic patients in the survival analysis, DCE-MRI was acquired

at baseline (in 26 patients), day -2 (21 patients), day 1 (21 patients), day 5 (24 patients), week 5 (27 patients), and week 10 (27 patients). The association between EFS as a continuous measure and each DCE-MRI parameter was examined. Lower week 10 measures of average K^{trans} was significantly associated with longer EFS ($P = 0.034$). An additional categorical analysis of the average K^{trans} at week 10 was performed using Kaplan–Meier curves stratified according to the median value for the cohort ($0.054 \, min^{-1}$). The group with average K^{trans} less than the median had a significantly higher EFS rate than the group with average K^{trans} larger than the median ($P = 0.037$ from a log-rank test).

The association between length of overall survival as a continuous measure and each DCE-MRI parameter was also examined. Three earlier parameters including the skewness of K^{trans} and v_e on day -2 and the skewness of v_p on day 1 were significantly associated with overall survival ($P = 0.044$, 0.039, and 0.043, respectively). Smaller skewness values were associated with longer survival. Lower mean v_e at week 10 was also significantly associated with longer survival ($P = 0.015$).

DISCUSSION

This study was the first to assess the impact of bevacizumab alone on tumour vasculature in pediatric OS. Average K^{trans} and v_p were both significantly lower than baseline values at 24 h (day -2) after the first administration of bevacizumab alone, demonstrating a sensitivity of OS vasculature to VEGF inhibition. These drops of K^{trans} and v_p may indicate a decrease in tumour permeability and tumour vessel density, and could be a sign of a transient 'normalisation'. This transient 'normalisation' decreases the tumour interstitial fluid pressure and improves tumour perfusion that consequently improves the drug delivery to tumour (Dickson et al, 2007). However, K^{trans} and v_p rapidly increased back to baseline levels at 72 h (day 1), demonstrating a relatively short optimal window for the addition of cytotoxic therapy. Measures of bevacizumab exposure were not significantly associated with changes in DCE-MRI parameters during this upfront window, but this analysis may have been limited by the small sample size of patients with pharmacokinetic data.

The serial DCE-MRI kinetic parameters during neoadjuvant therapy were compared with FDG-PET, explored for correlations with bevacizumab and MTX exposure, and evaluated for associations with clinical end points of histologic response and survival. The DCE-MRI parameters of K^{trans} and v_p were significantly lower than baseline at both the mid-point and end of neoadjuvant therapy. In addition, SUV_{max} was moderately correlated with v_p at week 5 and K^{trans} at week 5 and week 10 that may indicate that the impact of therapy on the integrity of the vasculature resulted in a corresponding decrease in tumour viability indicated by the decreased metabolism. The DCE-MRI and ^{18}F-FDG PET imaging provide complementary and consistent information for the evaluation of OS response. Although the cumulative radiation exposure from the three FDG PET CT scans was higher than allowable for radiation workers in a single year (30 vs 20 mSV), in the context of an often fatal disease treated with cytotoxic chemotherapy, we believe this is unlikely to have any clinical significance.

A decrease in v_p at the end of neoadjuvant therapy was correlated with increased exposure to both bevacizumab and MTX but was not associated with increased necrosis, longer EFS, or overall survival. This may indicate that although the addition of bevacizumab had an acute impact on v_p, it did not have an appreciable impact on clinical outcome. In contrast, a decrease in K^{trans} at week 5 was associated with increased MTX exposure and a smaller K^{trans} at week 10 was significantly associated with clinical

outcomes of greater percent necrosis, longer EFS, and overall survival. Only pharmacokinetic measures of MTX exposure were estimated in this study, and this is the central component of the neoadjuvant therapy with four high-dose courses administered at weeks 3, 4, 8, and 9. The other two components of therapy were cisplatin and doxorubicin that were administered in two cycles at week 0 and week 5 and may play a less significant role. The associations between imaging metrics and drug exposure are consistent with the pharmacological activity of bevacizumab binding VEGF-A to reduce and prevent angiogenesis, whereas cytotoxicity of chemotherapy drugs (MTX and so on) can cause vasculature cell death, resulting in necrosis.

The early effects of bevacizumab alone in clinical human trials have been rarely reported as it is usually administered concurrently with cytotoxic therapy (Hurwitz et al, 2004). In one human study, K^{trans} and v_p were reported to be significantly decreased in glioblastoma patients 24 h after the administration of bevacizumab (Port et al, 2010), consistent with our results in OS. In preclinical animal studies, permeability in DCE-MRI was reported to significantly decline 24 h after a single dose of bevacizumab in a human melanoma model (Cyran et al, 2013), but results in other studies 3 days after bevacizumab treatment in a breast xenograft model were inconsistent with increased v_p (Moestue et al, 2013) but decreased K^{trans} (Kim et al, 2011).

The DCE-MRI parameters have been associated with clinical outcome measures of histologic response and survival in other OS trials not incorporating antiangiogenic agents. One such trial found that lower k_{ep} at the completion of neoadjuvant therapy was significantly predictive of EFS (Reddick et al, 2001). This is very similar to the results in the current study in which a lower K^{trans} at week 10 was significantly associated with better EFS. In another study, the difference of v_e (extravascular, extracellular space) between the outer and inner halves of tumour at baseline was significantly associated with the EFS (Guo et al, 2012). In the current study, we found that none of the differences in DCE-MRI kinetic parameters between the outer and inner halves of tumour were significantly associated with EFS at any time point. This contradiction could be because of differences between the 2D single slice acquisition in the older study and the 3D acquisition (i.e., covering the entire tumour volume) used in this study. This contradiction could also be partially because of the different treatments that could lead to a different association between the imaging measures and EFS. Another consideration could be that the normalisation of the tumour vasculature by antiangiogenic therapy makes the tumour appear more homogeneous with reduced differences between the outer and inner halves of tumour at the later time points. It has been recognised, as shown in Buckley (2002), that the extended Tofts model with the vascular term can underestimate the true plasma volume. However, although acknowledging the limitations of the model used to analyse the data, the potential underestimations should be similar across the imaging data analysed and should not significantly impact the results of the associations demonstrated in this study.

In conclusion, this is the first study to demonstrate significant changes of the plasma volume fraction and vascular leakage in OS with bevacizumab alone. Although bevacizumab had an acute impact on v_p and increased exposure to both bevacizumab and MTX corresponded to decreased v_p at end of neoadjuvant therapy, these changes did not have an appreciable impact on the clinical outcome. However, increased MTX exposure was associated with decreased K^{trans} during neoadjuvant therapy and smaller K^{trans} before surgery was significantly associated with clinical outcomes of greater percent necrosis, longer EFS, and overall survival. These same DCE-MRI parameters were correlated with ^{18}F-FDG PET measures of tumour metabolism during neoadjuvant therapy, and this could provide complimentary information for understanding the underlying changes in tumour physiology and response to

therapy. The associations between imaging metrics and drug exposure are consistent with bevacizumab binding VEGF-A to reduce and prevent angiogenesis, whereas MTX cytotoxicity could cause vasculature cell death, resulting in increased necrosis. Although not directly seen in this limited sample size, it is believed that the combination of demonstrated associations between drug exposure and imaging metrics, and imaging metrics and patient survival, provide a compelling rationale for larger studies using DCE-MRI to assess vascular effects of neoadjuvant therapy in OS.

ACKNOWLEDGEMENTS

CONFLICT OF INTEREST

The authors declare no conflict of interest.

REFERENCES

Amit P, Patro DK, Basu D, Elangovan S, Parathasarathy V (2014) Role of dynamic MRI and clinical assessment in predicting histologic response to neoadjuvant chemotherapy in bone sarcomas. *Am J Clin Oncol* 37(4): 384–390.

Bacci G, Ferrari S, Longhi A, Perin S, Forni C, Fabbri N, Salduca N, Versari M, Smith KV (2001) Pattern of relapse in patients with osteosarcoma of the extremities treated with neoadjuvant chemotherapy. *Eur J Cancer* 37(1): 32–38.

Bajpai J, Gamnagatti S, Kumar R, Sreenivas V, Sharma MC, Khan SA, Rastogi S, Malhotra A, Safaya R, Bakhshi S (2011) Role of MRI in osteosarcoma for evaluation and prediction of chemotherapy response: correlation with histological necrosis. *Pediatr Radiol* 41(4): 441–450.

Bland JM, Altman DG (2004) The logrank test. *BMJ* 328(7447): 1073.

Buckley DL (2002) Uncertainty in the analysis of tracer kinetics using dynamic contrast-enhanced T-1-weighted MRI. *Magn Reson Med* 47(3): 601–606.

Cheon GJ, Kim MS, Lee JA, Lee SY, Cho WH, Song WS, Koh JS, Yoo JY, Oh DH, Shin DS, Jeon DG (2009) Prediction model of chemotherapy response in osteosarcoma by 18F-FDG PET and MRI. *J Nucl Med* 50(9): 1435–1440.

Cox DR (1972) Regression models and life-tables. *J R Stat Soc Ser B* 34: 187–220.

Cox DR (1975) Partial likelihood. *Biometrika* 62: 269–276.

Crews KR, Liu T, Rodriguez-Galindo C, Tan M, Meyer WH, Panetta JC, Link MP, Daw NC (2004) High-dose methotrexate pharmacokinetics and outcome of children and young adults with osteosarcoma. *Cancer* 100(8): 1724–1733.

Cyran CC, Fu Y, Rogut V, Chaopathomkul B, Wendland MF, Shames DM, Brasch RC (2013) Evaluation of a novel macromolecular cascade-polymer contrast medium for dynamic contrast-enhanced MRI monitoring of antiangiogenic bevacizumab therapy in a human melanoma model. *Acad Radiol* 20(10): 1256–1263.

Delong ER, Delong DM, Clarkepearson DI (1988) Comparing the areas under 2 or more correlated receiver operating characteristic curves - a nonparametric approach. *Biometrics* 44(3): 837–845.

Dickson PV, Hamner JB, Sims TL, Fraga CH, Ng CY, Rajasekeran S, Hagedorn NL, McCarville MB, Stewart CF, Davidoff AM (2007)

Bevacizumab-induced transient remodeling of the vasculature in neuroblastoma xenografts results in improved delivery and efficacy of systemically administered chemotherapy. *Clin Cancer Res* 13(13): 3942–3950.

Dyke JP, Panicek DM, Healey JH, Meyers PA, Huvos AG, Schwartz LH, Thaler HT, Tofts PS, Gorlick R, Koutcher JA, Ballon D (2003) Osteogenic and Ewing sarcomas: estimation of necrotic fraction during induction chemotherapy with dynamic contrast-enhanced MR imaging. *Radiology* 228(1): 271–278.

Guo J, Reddick WE, Glass JO, Ji Q, Billups CA, Wu J, Hoffer FA, Kaste SC, Jenkins JJ, Ortega Flores XC, Quintana J, Villarroel M, Daw NC (2012) Dynamic contrast-enhanced magnetic resonance imaging as a prognostic factor in predicting event-free and overall survival in pediatric patients with osteosarcoma. *Cancer* 118(15): 3776–3785.

Hawkins DS, Conrad 3rd EU, Butrynski JE, Schuetze SM, Eary JF (2009) [F-18]-fluorodeoxy-D-glucose-positron emission tomography response is associated with outcome for extremity osteosarcoma in children and young adults. *Cancer* 115(15): 3519–3525.

Hoang BH, Dyke JP, Koutcher JA, Huvos AG, Mizobuchi H, Mazza BA, Gorlick R, Healey JH (2004) VEGF expression in osteosarcoma correlates with vascular permeability by dynamic MRI. *Clin Orthop Relat Res* 426: 32–38.

Hurwitz H, Fehrenbacher L, Novotny W, Cartwright T, Hainsworth J, Heim W, Berlin J, Baron A, Griffing S, Holmgren E, Ferrara N, Fyfe G, Rogers B, Ross R, Kabbinavar F (2004) Bevacizumab plus irinotecan, fluorouracil, and leucovorin for metastatic colorectal cancer. *N Engl J Med* 350(23): 2335–2342.

Huvos AG, Rosen G, Marcove RC (1977) Primary osteogenic sarcoma: pathologic aspects in 20 patients after treatment with chemotherapy, en bloc resection, and prosthetic bone replacement. *Arch Pathol Lab Med* 101: 14–18.

Jain RK (2005a) Antiangiogenic therapy for cancer: current and emerging concepts. *Oncology* 19(4 Suppl 3): 7–16.

Jain RK (2005b) Normalization of tumor vasculature: an emerging concept in antiangiogenic therapy. *Science* 307(5706): 58–62.

Kaplan EL, Meier P (1958) Nonparametric estimation from incomplete observations. *J Amer Statist Assn* 53: 457–481.

Kim H, Folks KD, Guo L, Stockard CR, Fineberg NS, Grizzle WE, George JF, Buchsbaum DJ, Morgan DE, Zinn KR (2011) DCE-MRI detects early vascular response in breast tumor xenografts following anti-DR5 therapy. *Mol Imaging Biol* 13(1): 94–103.

Longhi A, Errani C, De Paolis M, Mercuri M, Bacci G (2006) Primary bone osteosarcoma in the pediatric age: state of the art. *Cancer Treat Rev* 32(6): 423–436.

Moestue SA, Huuse EM, Lindholm EM, Bofin A, Engebraaten O, Maelandsmo GM, Akslen LA, Gribbestad IS (2013) Low-molecular contrast agent dynamic contrast-enhanced (DCE)-MRI and diffusion-weighted (DW)-MRI in early assessment of bevacizumab treatment in breast cancer xenografts. *J Magn Reson Imaging* 38(5): 1043–1053.

Parker GJ, Roberts C, Macdonald A, Buonaccorsi GA, Cheung S, Buckley DL, Jackson A, Watson Y, Davies K, Jayson GC (2006) Experimentally-derived functional form for a population-averaged high-temporal-resolution arterial input function for dynamic contrast-enhanced MRI. *Magn Reson Med* 56(5): 993–1000.

Port RE, Bernstein LJ, Barboriak DP, Xu L, Roberts TP, van Bruggen N (2010) Noncompartmental kinetic analysis of DCE-MRI data from malignant tumors: Application to glioblastoma treated with bevacizumab. *Magn Reson Med* 64(2): 408–417.

Reddick WE, Taylor JS, Fletcher BD (1999) Dynamic MR imaging (DEMRI) of microcirculation in bone sarcoma. *J Magn Reson Imaging* 10(3): 277–285.

Reddick WE, Wang S-C, Xiong X, Glass JO, Wu S, Kaste SC, Pratt CB, Meyer WH, Fletcher BD (2001) Dynamic magnetic resonance imaging of regional contrast access as an additional prognostic factor in pediatric osteosarcoma. *Cancer* 91(12): 2230–2237.

Rosen G, Caparros B, Huvos AG, Kosloff C, Nirenberg A, Cacavio A, Marcove RC, Lane JM, Mehta B, Urban C (1982) Preoperative chemotherapy for osteogenic sarcoma: selection of postoperative adjuvant chemotherapy based on the response of the primary tumor to preoperative chemotherapy. *Cancer* 49: 1221–1230.

Rosen G, Marcove RC, Caparros B, Nirenberg A, Kosloff C, Huvos AG (1979) Primary osteogenic sarcoma: the rationale for preoperative chemotherapy and delayed surgery. *Cancer* 43(6): 2163–2177.

Shih T, Lindley C (2006) Bevacizumab: an angiogenesis inhibitor for the treatment of solid malignancies. *Clin Ther* **28**(11): 1779–1802.

Tofts PS, Brix G, Buckley DL, Evelhoch JL, Henderson E, Knopp MV, Larsson HBW, Lee T-Y, Mayr NA, Parker GJM, Port R, Taylor JS, Weisskoff RM (1999) Estimating kinetic parameters from dynamic contrast-enhanced T1-weighted MRI of a diffusible tracer: standardized quantities and symbols. *J Magn Reson Imaging* **10**(3): 223–232.

Tofts PS, Kermode AG (1991) Measurement of the blood-brain barrier permeability and leakage space using dynamic MR imaging. *Magn Reson Med* **17**(2): 357–367.

Turner DC, Navid F, Daw NC, Mao S, Wu J, Santana VM, Neel M, Rao B, Willert JR, Loeb DM, Harstead KE, Throm SL, Freeman 3rd BB, Stewart CF (2014) Population pharmacokinetics of bevacizumab in children with osteosarcoma: implications for dosing. *Clin Cancer Res* **20**(10): 2783–2792.

Verstraete KL, Lang P (2000) Bone and soft tissue tumors: the role of contrast agents for MR imaging. *Eur Radiol* **34**: 229–246.

Wilcoxon F (1945) Individual comparisons by ranking methods. *Biometrics* **1**(6): 80–83.

Wunder JS, Paulian G, Huvos AG, Heller G, Meyers PA, Healey JH (1998) The histological response to chemotherapy as a predictor of the oncological outcome of operative treatment of Ewing sarcoma. *J Bone Joint Surg Am* **80**(7): 1020–1033.

Ye Z, Zhu J, Tian M, Zhang H, Zhan H, Zhao C, Yang D, Li W, Lin N (2008) Response of osteogenic sarcoma to neoadjuvant therapy: evaluated by 18F-FDG-PET. *Ann Nucl Med* **22**(6): 475–480.